Molecular Motions and Ion Diffusions of the Room-Temperature Ionic Liquid 1,2-Dimethyl-3-propylimidazolium Bis(trifluoromethylsulfonyl)amide (DMPImTFSA) Studied by ^{1}H, ^{13}C, and ^{19}F NMR

Kikuko Hayamizu,*,† Seiji Tsuzuki,† and Shiro Seki‡

National Institute of Advanced Industrial Science and Technology (AIST), AIST Tsukuba Center 5, Tsukuba 305-8565, Japan, and Materials Science Research Laboratory, Central Research Institute of Electric Power Industry (CRIEPI), 2-11-1, Iwado-kita, Komae, Tokyo 201-8511, Japan

Received: March 19, 2008; Revised Manuscript Received: September 8, 2008

The diffusive properties of an imidazolium room-temperature ionic liquid (RTIL), 1,2-dimethyl-3-propylimidazolium bis(trifluoromethylsulfonyl)amide (DMPImTFSA), are studied from the ionic conductivity and the ion diffusion coefficients measured by pulsed field gradient spin echo NMR. The temperature-dependent ^{1}H, ^{19}F, and ^{13}C NMR spin−lattice relaxation time T_1 values were observed, and the ^{1}H T_1 for DMPIm showed T_1 minima for various protons. According to the Bloemberger−Purcell−Pound (BPP) equation, the correlation time τ_c values were directly calculated from ^{1}H NMR. By using the ^{1}H τ_c values, an evaluation of the ^{13}C T_1 was attempted for the carbons having protons. The τ_c estimated for molecular motions of DMPIm changes from 1.3 ns at 253 K to 72 ps at 353 K. The Stokes−Einstein−Debye (SED) model suggests that the τ_c is too short for the overall molecular reorientation near room temperature. Consequently, the possibility of small-angle molecular rotation is proposed and tentative flip angles are calculated by using the translational diffusion coefficient, the bulk viscosity measured in this study, and the τ_c obtained from ^{1}H T_1 data in the temperature range between 283 and 353 K. The flip amplitude increases with the temperature. DMPIm has isotropic reorientational motions with temperature-dependent amplitude, in addition to fast intramolecular motions such as methylene segmental motions, methyl rotational motion, and conformational exchange of the imidazolium ring. The existence of fast motions of TFSA is also shown. The translational diffusion of the ions is the slowest dynamic process in the present RTIL. Ab initio molecular orbital calculations are performed to understand the geometries of stable complexes of $DMPIm^{+}$ and $TFSA^{-}$, and the formation energies from the isolated ions are evaluated. The computed results are important for interpreting the ^{1}H T_1 behaviors observed for the imidazolium ring protons.

Introduction

Room-temperature ionic liquids (RTILs), which consist only of ions, have attracted much attention on account of their physical properties such as viscosity, vapor pressure, thermal transition temperature, and conductivity. Initially, studies were aimed at possible practical applications due to the desirable properties of the RTILs. Electrochemical aspects of ionic liquids[1] and physical properties have been reviewed,[2] and databases are now available through the Internet.[3] We have concentrated on measuring the temperature dependence of the self-diffusion coefficients (D) of the individual ions in neat[4−8] and binary RTILs[9,10] using ^{1}H, ^{19}F, and ^{7}Li (binary systems only) pulsed field gradient spin echo (PGSE) NMR methods together with other physicochemical properties. In most cases the cation diffuses a little faster than the counteranion and the difference is closely related to the relative molecular ion size. Recently, imidazolium cations with bulky side chains were reported to diffuse slower than the anion BF_4 in the ionic liquid state.[11] NMR measurements were also reported for pyrrolidinium IL binary systems including the frozen state.[12] The effects of pressure on the transport properties of $BMImPF_6$ (1-butyl-3-methylimidazolium hexafluorophosphate) were also reported.[13]

Diffusion coefficient measurements using pulsed field gradient (PFG) NMR were first performed by inserting two gradient pulses into a Hahn echo sequence (PGSE).[14] In systems where $T_2 < T_1$, the analogous stimulated echo based sequence (PGSTE) results in a better signal-to-noise ratio.[15] To minimize signal distortions resulting from eddy currents and background gradients, bipolar-gradient variants of the pulsed field gradient stimulated echo (BPGSTE) sequence were proposed.[16] When the target species is a small and rapidly diffusing molecule like water, the gradient amplitudes used are small (<1 T/m) and various pulse sequences are possible to minimize the artifacts induced by application of the PFGs. However, generally, RTILs have high viscosities and the diffusion coefficients are much smaller than those of the usual liquid samples. Consequently, larger gradient amplitudes (up to ∼15 T/m) are required to provide sufficient signal attenuation to ensure accurate diffusion measurements. Such high gradient amplitudes can lead to artifactual attenuation.[17] High amplitude bipolar gradient pulses are more demanding of the gradient generation hardware than the equivalent monopolar pulses and are consequently more likely to lead to artifactual attenuation due to mismatched gradient pulse pairs.

* To whom correspondence should be addressed. Telephone/fax: +81-29-861-6295. E-mail: hayamizu.k@aist.go.jp.
† AIST.
‡ CRIEPI.

10.1021/jp802392t CCC: $40.75
Published on Web 10/31/2008

Since RTILs are liquids with specific properties, molecular motions and interactions between ions have been studied widely by spectroscopic and computational methods. Especially the NMR spin−lattice relaxation time T_1 can afford information on intramolecular, reorientational, or flip motions, and the time scale is related to the measuring NMR frequency. ^{13}C relaxation times have been studied for the imidazolium cation ionic liquids to understand the molecular motions.[18−22] The ^1H and ^{19}F relaxation times were reported for the RTILs of imidazolium cations having bulky chains.[11] Generally, in the extreme narrowing condition, the ^1H T_1 in the liquid state increases linearly with increasing temperature. On the other hand, in the solid state the temperature dependence of the ^1H T_1 exhibits minima for molecular motions, and many such studies have been made mainly before the introduction of high-resolution solid-state NMR techniques. We have reported that in viscous liquids a ^1H T_1 minimum can be observed for small molecules in doped electrolytes consisting of ethylene glycol dimethyl ethers ($CH_3O(CH_2CH_2O)_nCH_3$ ($n = 3-5$)) with a lithium salt and neat liquid polyethylene glycol dimethyl ethers of molecular weights 400 and larger.[23] The ^1H relaxation mechanism can be interpreted as resulting from fast segmental motions of the $-OCH_2CH_2-$ moiety. Also, the protons in hydrated and anhydrous phosphoric acids showed a ^1H T_1 minimum and the correlation times were evaluated for proton one-jump motions at various temperatures for the various phosphoric acid concentrations.[24] Since ^1H NMR relaxation is dominated by dipole−dipole interactions, reorientational correlation times can calculated from the minimum T_1 by using the Bloemberge−Purcell−Pound (BPP) equation.[25] We also reported the ^1H, ^{19}F, and ^7Li NMR of the neat and doped quaternary ammonium RTIL, *N*,*N*-diethyl-*N*-methyl-*N*-(2-methoxyethyl) ammonium bis(trifluoromethylsulfonyl)amide (DEME-TFSA), where T_1 minima were observed for the ^1H and ^7Li resonances.[10]

In the present paper, the imidazolium ionic liquid 1,2-dimethyl-3-propylimidazolium bis(trifluoromethylsulfonyl)amide (DMPImTFSA) is the target ionic liquid, where three different CH_3 groups exist including $N-CH_3$, $C-CH_3$, and terminal CH_3 in the propyl chain. The C_2 position of the

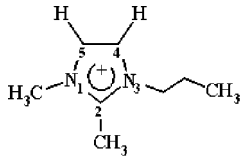

DMPIm

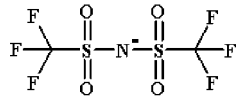

TFSA

imidazolium ring is substituted by CH_3 for the reduction of the hydrogen bonding. In Chart 1, the stable molecular structures of isolated DMPIm and TFSA are shown from the ab initio molecular orbital calculations. We have already examined the properties of DMPImTFSA for use as a low-flammable and low-volatile electrolyte in lithium secondary batteries.[26,27]

The self-diffusion coefficients of the DMPIm and TFSA are determined from the ^1H and ^{19}F resonances, respectively, and will be discussed in connection with the ionic conductivity. The ^1H, ^{13}C, and ^{19}F NMR T_1 values were also obtained. The ^1H signals of the three methyl and two methylene groups showed T_1 minima. In the liquid state, the ^{19}F T_1 of the CF_3 of TFSA became longer as the temperature increased without a minimum being observed. Since the predominant relaxation mechanism of ^1H NMR is the $^1H-^1H$ dipole interactions, the correlation times were calculated from the T_1 minimum value using the well-known Bloemberger−Purcell−Pound (BPP) equation. Isotropic molecular reorientational motion is assumed together with the intramolecular motions. Since the relaxation of the ^{13}C resonances is known to be influenced by $^1H-^{13}C$ dipolar interaction, ^{13}C chemical shift anisotropy, and spin−rotation interactions, the analysis of the ^{13}C T_1 is usually complex. In this paper, using the ^1H correlation times the $^1H-^{13}C$ dipolar interaction term of the ^{13}C T_1 was calculated and compared with the observed values. A brief discussion will be made about the Stokes−Einstein (SE) and Stokes−Einstein−Debye (SED) equations for the present ionic liquid of DMPImTFSA. We propose that the correlation time obtained from the ^1H T_1 is related to small-angle isotropic molecular reorientational motion, and the angles for the reorientation motion in the temperature range studied were estimated. To clarify the cation−anion interaction scheme, ab initio molecular orbital calculations were performed for the DMPImTFSA complex. The spatial positions for the anion are important for understanding the short T_1 of the imidazolium ring protons and CF_3 at low temperature.

Room-temperature ionic liquids are new materials for which the classical equations are clearly too simple and sophisticated theory is necessary to interpret thoroughly the specific properties of RTILs. In this paper we intend to measure precise experimental data of DMPImTFSA and to understand the molecular motions, intermolecular interactions, and diffusive phenomena by using the classical equations and by ab initio molecular orbital calculations.

Experimental Section

Sample Preparation. 1,2-Dimethyl-3-propylimidazolium bis(trifluoromethylsulfonyl)amide (DMPImTFSA) was purchased from Aldrich-Fluka, dried in a vacuum chamber at 323 K for more than 24 h, and stored in a dry argon-filled glovebox ($[O_2] < 0.4$ ppm, $[H_2O] < 0.1$ ppm; Miwa Mfg Co., Ltd.). For NMR diffusion measurements, the samples were placed in a 5-mm NMR microtube (BMS-005J, Shigemi, Tokyo) to a height of 5 mm and sealed with epoxide resin with argon atmosphere to prevent moisture. The magnetic susceptibility of the sample tube is matched to the sample, thereby affording good magnetic homogeneity over the whole sample volume. The sample volume and the field homogeneity are known to affect significantly the diffusion coefficient measured.[28] The length of the sample was intentionally made short so that it lay within the constant region of the applied magnetic gradient, and the use of short samples also minimized the likelihood of convection effects.[29] Annat et al. reported intrinsic internal gradients in ILs,[30] but we did not reproduce their experimental results under proper sample conditions and the details will be published elsewhere. For the ^{13}C NMR measurements, a usual 5-mm NMR sample tube with a height of 40 mm was used to improve the sensitivity.

Ionic Conductivity Measurements. The temperature dependence of the ionic conductivity of the DMPImTFSA was measured in SUS/electrolyte/SUS symmetric blocking cells and determined by the complex impedance method, using a Princeton Applied Research PARSTAT-2263 ac impedance analyzer, in the frequency range 200 kHz−50 mHz with an applied voltage of 10 mV over the temperature range 353−233 K with cooling.

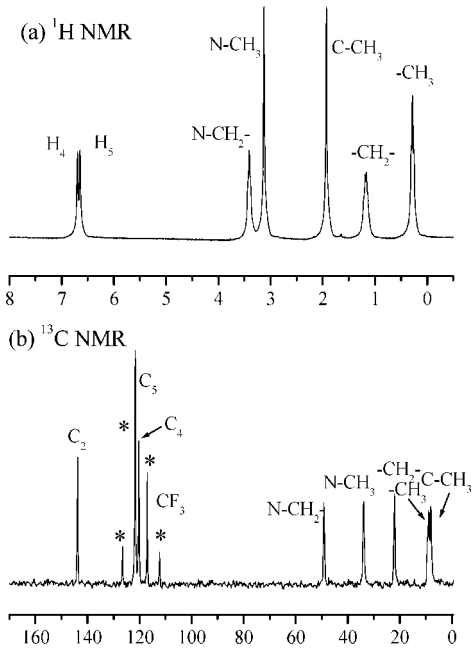

Figure 1. (a) ^{1}H and (b) ^{13}C NMR spectra of DMPImTFSA. The assignment of the ^{13}C NMR spectrum was determined from the ^{1}H undecoupled spectrum. The asterisks denote the CF_3 quartet signals of TFSA.

Viscosity Measurements. The temperature dependence of viscosity of the DMPImTFSA was measured with a Stabinger-type viscometer (Anton Paar) in the temperature range 353−283 K with cooling.

NMR Measurements. All NMR spectra were measured on a Tecmag Apollo with a 6.35 T wide bore magnet using JEOL probes and controlled by a JEOL console. The T_1 measurements were performed by the inversion recovery (180°−τ−90°−Acq) sequence. Broad-band ^{1}H decoupling was used in the ^{13}C NMR measurements. The ^{1}H and ^{13}C NMR spectra of the DMPIm were measured at 270.17 and 67.94 MHz, respectively, and are shown in Figure 1 with spectral assignments. The ^{19}F NMR spectra of CF_3 of TFSA were observed at 254.19 MHz. All measurements were performed without sample spinning to prevent disturbance from sample motion.

A modified Hahn spin echo based sequence incorporating a gradient pulse in each τ period (PGSE) was used to measure the diffusion coefficients, where the T_2 values were long to afford good echo signals. The echo attenuation, E, is related to the experimental variables and the diffusion coefficient D by

$$E = \exp(-\gamma^2 g^2 \delta^2 D(\Delta - \delta/3)) \quad (1)$$

where g is the strength of the gradient pulse of duration δ, and Δ is the interval between the leading edges of the gradient pulses.[14] The gradient strength was calibrated by using H_2O and D_2O (^{2}H NMR).[31] The maximum g used was 10 T/m, and the longest δ was 2 ms. The measurements were performed by holding g constant and varying δ for more than 15 points with setting the repetition time for a 5 times longer T_1. Δ defines the time scale of diffusion measurement, and in a homogeneous system D is independent of Δ. A single exponential diffusion plot following eq 1 indicates free diffusion. However, above ambient temperature with a longer sample height like 5 mm and longer interval times Δ, the diffusion measurements are more prone to convection artifacts, leading to Δ dependence of the measured diffusion coefficients (larger apparent D for longer Δ).[29] At lower temperatures, as described in detail below, the apparent D values are dependent on Δ and become larger for shorter Δ, which is opposite to the convection effects. The measurements were made for two or three different Δ values, with Δ being set between 20 and 70 ms in the temperature range from 353 to 253 K with a cooling process by the flow method. At low temperatures a longer Δ is desirable for obtaining equilibrium values. Reasonable D values (free from the convection artifacts at higher temperatures and equilibrium values at low temperatures) were obtained for the proper Δ at every temperature. The measurements of the ^{1}H and ^{19}F NMR frequencies for the individual nuclei have been made simultaneously at a set temperature to exclude the possibility of a thermal history.

Computational Methods. The Gaussian 03 program[32] was used for the ab initio molecular orbital calculations. The basis sets implemented in the Gaussian program were used. Electron correlation was accounted for at the MP2 level.[33,34] The geometry of the complex was fully optimized at the HF/6-311G** level. The MP2 level interaction energy (E_{MP2}) was calculated by the supermolecule method. The basis set superposition error (BSSE)[35] was corrected in interaction energy calculations using the counterpoise method.[36] The formation energy of the complex from isolated ions (E_{form}) was calculated as the sum of the E_{MP2} and deformation energy (E_{def}), which is the sum of the increases in energies of DMPIm and TFSA by deformation of geometries in complex formation. In our earlier work, we evaluated the effects of choice of basis set and electron correlation correction on the calculated interaction energy of the 1-ethyl-3-methylimidazolium tetrafluoroborate complex.[37] The calculations show that the choice of basis set effects are negligible if the 6-311G** or a larger basis set is used and the effects of electron correlation beyond MP2 are very small. Therefore we studied the interaction energy for the ion pair at the MP2/6-311G** level in this work.

Results

Ionic Conductivity and Diffusion Coefficients of the Individual Ions. At 303 K the D values of DMPIm and TFSA were independent of Δ and indicated homogeneous environments for cation and anion. With decreasing temperature, a Δ dependence of the apparent D values was observed. As an example, the diffusion attenuation plots for DMPIm and TFSA acquired at 258 K are shown in Figure 2 by varying the time interval Δ. Although each plot is a single exponential, the decay increased as Δ became shorter. The apparent D value approached an equilibrium value at longer Δ. Generally, such time-dependent diffusion coefficients are referred to as anomalous diffusion and are commonly observed in fractal-like polymers[38,39] and porous media.[40] We have observed and reported these phenomena for the anion diffusion in poly(ethylene oxide) (PEO) type electrolytes,[41−43] and we indicated that the equilibrium diffusion coefficient correlates to the ionic conductivity. The diffusion of the countercation (i.e., lithium ion) is very slow or restricted, so it makes at best a small contribution to the ionic conductivity in the PEO-type electrolytes. Ionic liquids are viscous liquids and do not have solid structures like polymers and/or porous materials. In the present experiments time-dependent diffusion was observed only at low temperatures and provides good evidence for the increase of mutual interactions between the ions with decreasing temperature. The mutual interactions may obstruct the motion of the ions preventing isotropic diffusion, and the detailed analysis of the time-dependent diffusion coefficients is necessary to understand dynamic ionic interactions.

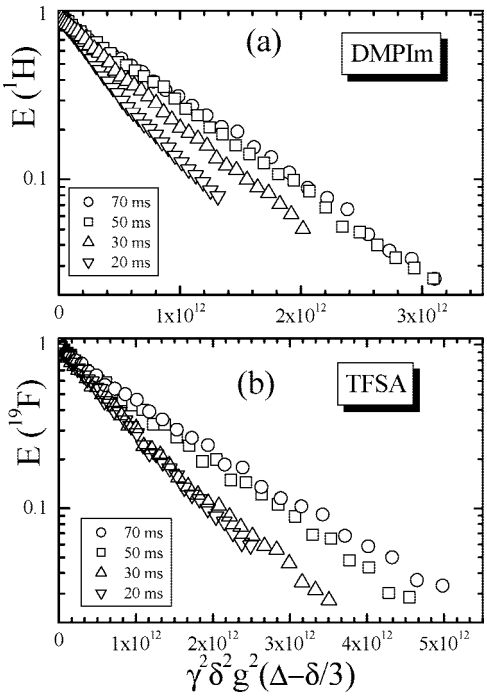

Figure 2. PGSE attenuation plots of (a) DMPIm (apparent D values of 8.60×10^{-13}, 6.34×10^{-13}, 5.25×10^{-13}, and 5.05×10^{-13} m^2 s^{-1}) and (b) TFSA (apparent D values of 5.10×10^{-13}, 4.50×10^{-13}, 3.37×10^{-13}, and 3.01×10^{-13} m^2 s^{-1}) for Δ of 20, 30, 50 and 70 ms, respectively at 258 K. The correlation coefficient (R^2) was better than 0.997 for each plot.

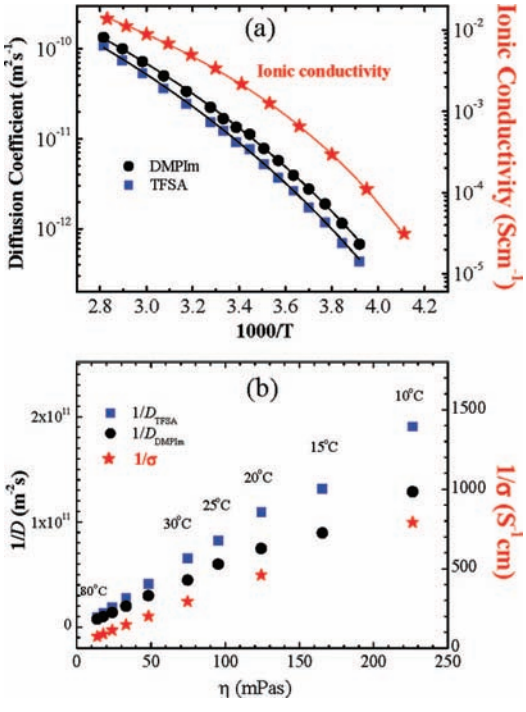

Figure 3. (a) Self-diffusion coefficients versus temperature for DMPIm (circles) and TFSA (squares), and temperature-dependent ionic conductivity for DMPImTFSA. The lines represent fits using the VFT relation. The fitting parameters are D_0, 2.16 ($\pm$0.03) and 3.60 ($\pm$0.05) $\times 10^{-8}$ m^{2}s^{-1}; B, 1071 ($\pm$65) and 1219 ($\pm$80) 1/K; and T_0, 151 ($\pm$4) and 145 ($\pm$5) K for DMPIm and TFSA, respectively. Similarly, assuming a VFT relationship for the ionic conductivity gave σ_0, 0.525 ($\pm$0.072) S cm^{-1}; B, 639 ($\pm$17) 1/K; and T_0, 178 ($\pm$1) K. (b) Reciprocals of D_{DMPIm}, D_{TFSA}, and σ plotted versus viscosity.

The D values are plotted versus temperature in Figure 3a, obtained by the measurements of "minimum convection effects" in the high-temperature region and "long time" in the low-temperature region. The Arrhenius plots of the D values in Figure 3a are curved and consistent with a Vogel−Fulcher−Tammann (VFT) type relationship (i.e., $D = D_0 \exp(-B/(T - T_0))$, where B, D_0, and T_0 are the fitting parameters) as shown in Figure 3a. The slopes of the plots were somewhat discontinuous around 288 K, and the activation energies calculated above and below 288 K are summarized in Table 1. The thermal activation energy for the translational diffusion is much smaller in the higher temperature range. The DMPIm diffuses faster than TFSA and the activation energies of DMPIm are a little smaller than those of TFSA in both temperature ranges.

TABLE 1: Activation Energies (kJ/mol) for Diffusive Properties

	above 288 K	below 288 K
ionic conductivity	26.2 ± 1.0	−
DMPrIm diffusion	33.6 ± 0.4	48.2 ± 0.9
TFSA diffusion	35.3 ± 0.4	49.9 ± 0.8

Figure 3a includes the Arrhenius plot of the ionic conductivity σ, and the curvature is considerable. The VFT-type fitting is also shown in the figure. The activation energy for the linear part of the ionic conductivity (i.e., migration of charged anions and cations) above 303 K was 26.2 kJ/mol (in Table 1) and was much smaller than those of the D values in the same temperature range (about 34 kJ/mol). Since NMR diffusion measurements cannot distinguish between the charged and paired (without charge) ions, in the higher temperature range the thermal activation of translational migration of the charged ions measured electrochemically is smaller than that determined from NMR translational diffusion measurements which include the paired ions.

The Stokes−Einstein (SE) equation for relating the diffusion coefficient to the viscosity (η) is given by

$$D = \frac{kT}{c\pi\eta a} \tag{2}$$

where a is the Stokes radius for the diffusing species and the constant c ranges between 4 and 6 for the slip and stick boundary conditions, respectively. Then, attempts were made to plot reciprocals of diffusion coefficients and ionic conductivity versus viscosity in Figure 3b. The viscosity changes from 13.9 (80 °C), to 95.4 (25 °C), to 226 (10 °C) mPa s, and linear relationships of the viscosity with $1/D_{\mathrm{TFSA}}$, $1/D_{\mathrm{MPrIm}}$, and $1/\sigma$ are shown, respectively.

For a species with a, the correlation time τ of the translational diffusion can be estimated from $\tau = 2a^2/D$.[44] Here we assume that the Stokes radius can be replaced by the van der Waals radius calculated from the molecular volume and 0.330 nm for DMPIm.[45] Strictly speaking, although the shape of DMPIm is not spherically symmetric, the SE relation is to a first approximation valid.[46] The estimated τ values were 1.6, 9.2, and 55 ns for 353, 303, and 273 K, respectively.

^{1}H and ^{19}F Spin−Lattice Relaxation. In Figure 4, the ^{1}H and ^{19}F T_1 values are plotted versus temperature. Except for the imidazolium ring protons and the CF_3 of TFSA, the ^{1}H T_1 values of N_1-CH_3, C_2-CH_3, and the α-CH_2, β-CH_2, and γ-CH_3 in the propyl group at the N_3 position showed T_1 minima. The ^{1}H and ^{19}F spin−lattice relaxation data were analyzed using the Bloembergen−Purcell−Pound (BPP) equation.[25]

$$\frac{1}{T_1} = C\sum_j \frac{1}{r_j^6}\left(\frac{\tau_c}{1+\omega_o^2\tau_c^2} + \frac{4\tau_c}{1+4\omega_o^2\tau_c^2}\right) \tag{3}$$

where ω_o is the observed frequency (rad s^{-1}), τ_c is the

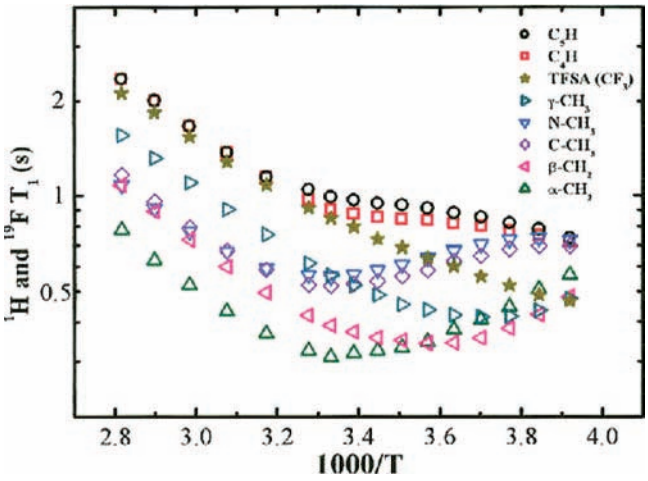

Figure 4. Temperature dependences of ^{1}H (DMPIm) and ^{19}F (TFSA) NMR T_1 values.

reorientational correlation time of the dipolar interaction, and the summation index j is over all interacting dipoles. Due to the term in parentheses in eq 3 the spin−lattice relaxation time is a minimum when $\omega_o\tau_c = 2\pi\nu_o\tau_c = 0.616$. In the current study the ^{1}H observed frequency, ν_o, is 270.17 MHz and τ_c is simply calculated to be 3.63×10^{-10} s (363 ps). The correlation times of the translational diffusion calculated above are 1 order longer (that is, translational diffusion is much slower) and thus do not contribute to spin−lattice relaxation mechanisms. C is calculated from the T_1 value observed at the minimum point. Thus eq 3 can be used to calculate τ_c from the T_1 values observed at any temperature. The τ_c values calculated are plotted versus temperature in Figure 5 for the proton signals having T_1 minima. The activation energies calculated from the linear parts in the higher temperatures are summarized in Table 2. The Arrhenius plots of α-CH_2, β-CH_2, and γ-CH_3 in the propyl group were all linear in the present temperature range, suggesting that a dominant relaxation process exists in the ^{1}H relaxation. The additional relaxation mechanisms are effective at the shorter τ_c values of β-CH_2 and terminal γ-CH_3 relative to α-CH_2 such as segmental and free rotational motions, respectively. The experimental results suggest that the τ_c obtained from BPP analysis can be written as

$$\frac{1}{\tau_c} = \frac{1}{\tau_o} + \frac{1}{\tau_s} \tag{4}$$

where τ_o and τ_s are the correlation times for the isotropic

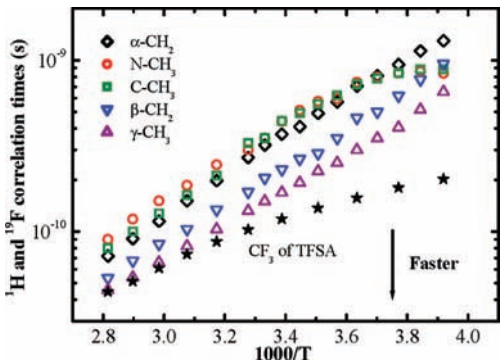

Figure 5. Correlation times of the three methyl and two CH_2 signals of DMPIm calculated from the T_1 minima and the CF_3 of TFSA calculated under the assumption that the extreme narrowing condition holds for the free rotation around the three symmetric axes.

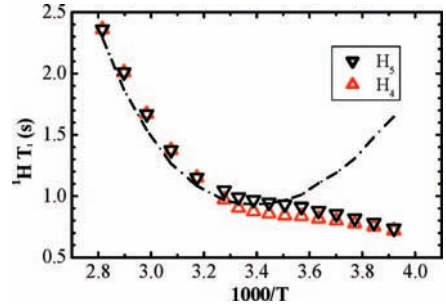

Figure 6. Observed T_1 values of the imidazolium ring protons for C_4H (upward-pointing triangles) and C_5H (downward-pointing triangles) and T_1 values calculated using correlation times of α-CH_2 of the propyl chain (dashed line).

molecular reorientation and intramolecular motions, respectively. As shown in Figure 5, the τ_c values of the two α-CH_3 groups at the N_1 and C_2 positions and α-CH_2 at the N_3 position of the imidazolium ring are, within experimental error, almost the same. A little spread between the three τ_c values at the higher temperature and deviations resulting from the faster motions of the two methyl groups from CH_2 were observed at temperatures below 273 K. As is well-known, fast segmental motions or rotational motions around the three axes of the CH_3 group are averaged out at the lower temperatures in the solid state; the important ^{1}H T_1 processes having the minima in the liquid state should be the reorientational motions of the whole molecule. Since the Arrhenius plot of the τ_c of the α-CH_2 is linear and corresponds to a single process, hereafter we assume that the τ_c of the α-CH_2 represents the correlation time of the whole molecule in the present temperature range.

For the ^{1}H T_1, C in eq 3 can be written as

$$C = \frac{3}{10}\gamma_i^4\hbar^2\sum_j \frac{1}{r_j^6} \tag{5}$$

where γ_i is the gyromagnetic ratio of ^{1}H, $\hbar$ is the reduced Planck constant, and r is the separation between dipoles (e.g., the H−H distance); the summation of the r^{-6} term is necessary for all neighboring protons. It is possible to sum the internal H−H distances for the imidazolium protons of C_4-H and C_5-H by using the optimized geometry from molecular orbital calculations. Then the calculation of the ^{1}H T_1 for the ring proton C_5H near the N−CH_3 (not N−$CH_2CH_2CH_3$) was made as shown in Figure 6 by using the τ_c of the α-CH_2. Here the H−H distances between C_5-H and CH_3 are included. Clearly, above 303 K the calculated T_1 for the imidazolium C_5-H agreed with the observed T_1 values of the C_4-H and C_5-H, of which the T_1 values were almost the same. As the temperature decreased, the observed

TABLE 2: Activation Energies (kJ/mol) for Local Motions Obtained from the Arrhenius Plots of τ_c (Figure 5) or T_1 (Figure 4)

	E_a (kJ/mol)	temp range (K)	
α-CH_2 (in propyl)	22.0 ± 0.5	353−253	from τ_c
β-CH_2 (in propyl)	21.2 ± 0.3	353−253	from τ_c
γ-CH_3 (in propyl)	19.6 ± 0.2	353−253	from τ_c
C−CH_3	24.1 ± 0.5	353−283	from τ_c
N−CH_3	19.1 ± 0.4	353−283	from τ_c
H_4	16.9 ± 0.3	353−313	from T_1
	3.7 ± 0.2	303−253	
H_5	16.9 ± 0.3	353−313	from T_1
	2.7 ± 0.1	303−253	
CF_3	15.9 ± 0.3	353−313	from T_1
	8.9 ± 0.2	303−253	

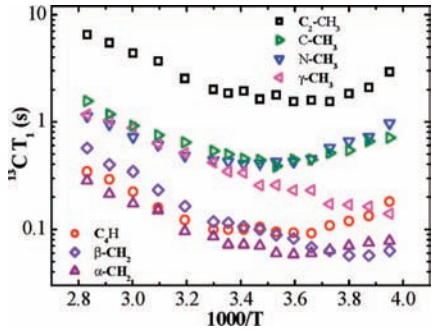

Figure 7. Arrhenius plots of observed ^{13}C T_1 values for each carbon of DMPImTFSA. The C_5 signal was overlapped with a signal of the CF_3 quartet.

T_1 values became shorter as additional fast relaxation mechanisms become operative.

For the ^{19}F T_1 resulting from the internal rotation around the three symmetrical axes of the CF_3 of TFSA, C can be written from eq 5 as follows:

$$C = \frac{9}{20}\gamma_F{}^4\hbar^2\frac{1}{r^6} \tag{6}$$

where r is the F−F atomic distance in CF_3 and γ_F is the ^{19}F gyromagnetic ratio. Since the ^{19}F T_1 became longer as the temperature increased without minimum, the extreme narrowing condition (i.e., $\omega_o\tau_c \ll 1$) may be assumed. Thus for the CF_3 group eq 3 becomes

$$\frac{1}{T_1} = \frac{9}{4}\gamma_F{}^4\hbar^2\frac{1}{r^6}\tau_c \tag{7}$$

A somewhat curved Arrhenius plot of the ^{19}F correlation times calculated using eq 7 is given in Figure 5. It is uncertain whether the relaxation processes correspond to either the internal rotation of the CF_3 or the molecular reorientation of TFSA. The rate of the motion was a little faster than the DMPIm at the higher temperatures, and became much faster at the lower temperature.

^{13}C Resonance Spin−Lattice Relaxation. Arrhenius plots of the ^{13}C T_1 for all carbons of DMPImTFSA are shown in Figure 7. The quaternary carbon C_2 in the imidazolium ring had the longest T_1 and the protonated C_4 (the C_5 was not observed due to overlapping with an intense signal of the CF_3 quartet) had a shorter T_1. The ^{13}C T_1 values of α-methyl carbons at the N_1 and C_2 positions behaved similarly at all temperatures. The T_1 values of the terminal CH_3 in the propyl group were similar to the α-methyl carbons in the higher temperature region, while the T_1 became shorter at lower temperatures similar to the β-CH_2. The present behaviors of the temperature dependences of ^{13}C T_1 values of DMPImTFSA resemble those of 1-butyl-3-methyl- and 1-ethyl-3-methylimidazolium ionic liquids.[18−22] Although the ^{13}C T_1 minima can be observed for many carbons, the procedure used for analyzing the ^{1}H T_1 data cannot be adopted to calculate the correlation times.

The ^{13}C NMR spin−lattice relaxation is dominated by the ^{1}H−^{13}C dipole−dipole relaxation mechanism. Chemical shift anisotropy and the spin−rotation interactions (mainly CH_3) are also known to be important mechanisms.[47] The conventional method for interpreting the ^{13}C T_1 data is to measure the nuclear Overhauser effect (NOE) to estimate the contribution of the dipolar relaxation mechanism to the ^{13}C T_1 as reported for the RTILs.[18−22]

Generally, the dipole−dipole relaxation time, $T_1{}^{dd}$, between unlike spins A and X (heteronuclear interaction) can be expressed in terms of the spectral density function $J(\omega)$.[47]

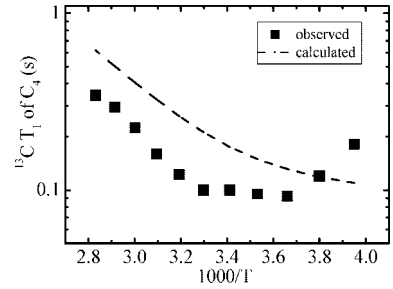

Figure 8. ^{13}C T_1 values of the imidazolium C_4 carbon having a proton, observed (squares) and calculated (solid line) using eq 10, where r_{CH} = 0.1093 nm and the τ_c of α-CH_2 obtained by ^{1}H NMR.

$$\frac{1}{T_1^{dd}}(X) = \frac{2}{15}\gamma_X{}^2\gamma_A{}^2\hbar^2 I_A(I_A+1)\sum_j r_j^{-6}(J(\omega_A-\omega_X) + 3J(\omega_X) + 6J(\omega_A+\omega_X)) \tag{8}$$

The dipole−dipole contribution to the T_1 of ^{13}C NMR from the protons (I_A = 1/2) can be expressed as

$$\frac{1}{T_1^{dd}}(^{13}C) = \frac{2}{15}\gamma_C{}^2\gamma_H{}^2\hbar^2 I_H(I_H+1)\sum_j r_j^{-6}(J(\omega_H-\omega_C) + 3J(\omega_C) + 6J(\omega_H+\omega_C)) \tag{9}$$

When the dipolar relaxation process of a carbon is induced mainly by the protons attached to the carbon and the number of the protons is n, eq 9 can be rewritten as

$$\frac{1}{T_1^{dd}}(^{13}C) = \frac{n}{10}\left(\gamma_C\gamma_H\hbar\left\langle\frac{1}{r^3}\right\rangle\right)^2\left(\frac{1}{1+\tau_c{}^2(\omega_H-\omega_C)^2} + \frac{3}{1+\tau_c{}^2\omega_C{}^2} + \frac{6}{1+\tau_c{}^2(\omega_H+\omega_C)^2}\right)\tau_c \tag{10}$$

where r is the C−H bond length, τ_c is the correlation time for the motions of the C−H axis, and ω_C and ω_H (rad s^{-1}) are the ^{13}C and ^{1}H NMR resonance frequencies, respectively.

An attempt was made to calculate the ^{13}C T_1 values by using eq 10 from the correlation times obtained by the ^{1}H T_1 data. Here we tried to calculate the ^{13}C T_1 of the imidazolium carbons having a proton (C_4 or C_5) under the assumption that the imidazolium ring reorientation takes place with the τ_c of the α-CH_2 derived from the ^{1}H NMR measurements. The calculated ^{13}C T_1 values of the C_4 are shown in Figure 8 together with the observed ones. The calculated T_1 values are longer than the observed ones at higher temperatures, and additional ^{13}C relaxation processes are clearly operative. At low temperatures, the calculated ^{13}C T_1 values are shorter than the observed ones and are quite different from ^{1}H T_1 of the ring protons in Figure 6. The discrepancy is acceptable because precise NOE measurements were not made in the present paper and also broad-band ^{1}H decoupling may affect the ^{13}C T_1 values. The calculated relaxation rate was about 55% of the observed one above 303 K. However, it is certain that similar reorientational motions affect the T_1 values of the imidazolium ring in ^{1}H and ^{13}C resonances.

The ^{13}C T_1 values of methyl carbons of the N-CH_3 and C-CH_3 are longer as shown in Figure 7. The calculated ^{13}C T_1 values from the corresponding τ_c values in the ^{1}H NMR are much shorter and are about 1/7 of the observed one in the high-temperature range. As is well-known, the ^{13}C T_1 values of methyl carbons are affected by the C−H dipolar interactions resulting from rotation around the three symmetrical axes in the liquid state, which brings the much longer ^{13}C T_1 values.

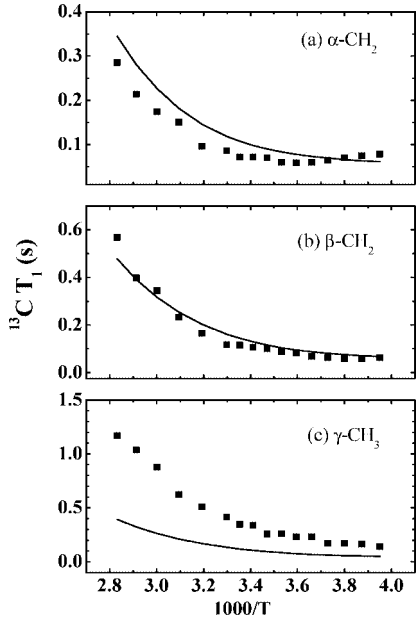

Figure 9. ^{13}C T_1 values of (a) α-CH_2, (b) β-CH_2, and (c) γ-CH_3 in the propyl group, observed (squares) and calculated (solid lines) by using eq 10 and individual correlation times of the protons obtained by ^1H NMR.

The ^{13}C T_1 of the propyl carbons in the present RTIL showed a general trend of the liquid-state NMR, such as a longer T_1 by approaching an alkyl terminal. The calculations of the ^{13}C T_1 for the propyl carbons were tried for each carbon by using eq 10 and are shown in Figure 9. The calculated ^{13}C T_1 for the α-CH_2 was a little longer than the observed ones at each temperature. The better agreement in the ^{13}C T_1 values of the β-CH_2 was a little fortuitous. Clearly the observed ^{13}C T_1 values for the γ-CH_3 were much longer than the calculated values by a ratio of about 3:1 over the whole temperature range, and the smaller discrepancy among the three methyl carbons is due to the shorter ^1H τ_c of the terminal methyl shown in Figure 5. Clearly the spin−rotational ^{13}C relaxation mechanism reduces the dipole−dipole interaction effects in the CH_3 groups. Although the ^{13}C T_1 values for the carbons estimated using the τ_c value derived from the ^1H T_1 are inaccurate, it is sure that the correlation times obtained from the T_1 minimum of the ^1H NMR can be used to interpret the $^1H-^{13}C$ dipole−dipole contribution to the ^{13}C T_1.

Geometries and Interaction Energies for DMPIm Complex with TFSA. To estimate the contribution of the intermolecular dipole−dipole interactions to the relaxation process, the interaction energy for the DMPIm complex with TFSA was calculated using the ab initio molecular orbital method. Before calculating the DMPImTFSA complex, we optimized the geometries of the DMPImCl complex to reveal the stable positions of an anion around the DMPIm. The DMPImCl complex was optimized from 20 initial geometries. The five local minima shown in Figure 10 were determined from the geometry optimizations. The E_{form} values for two geometries **1a** and **1b** (−86.7 and −85.8 kcal/mol, respectively) are larger (more negative) than those for **1c**−**1e** (−73.3 to −79.6 kcal/mol). The Cl^- is above or below the plane of the imidazolium ring in the geometries **1a** and **1b**. The distance between C_2 and Cl^- in **1a** and **1b** is 3.04 and 2.96 Å, respectively, while the Cl^- has close contact with the C_4-H or C_5-H in **1c**−**1e**. The calculated interaction energies show that the Cl^- prefers to have close contact with the C_2. The same preference was reported

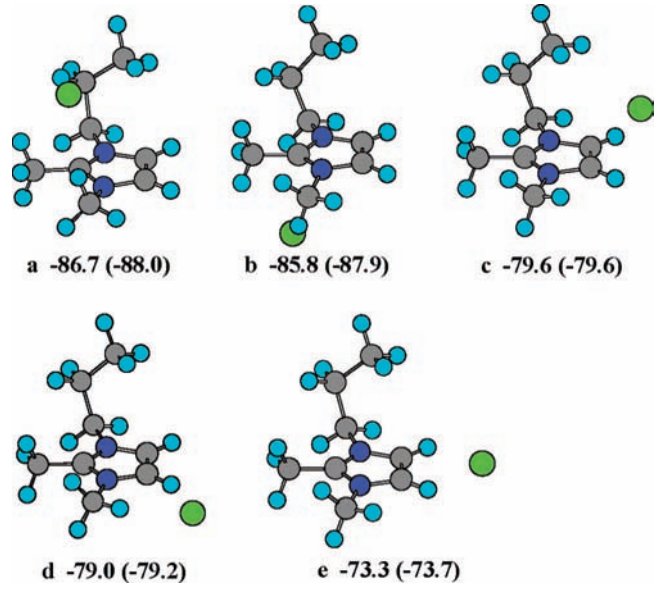

Figure 10. HF/6-311G** level optimized geometries and formation energies [$E_{form} = E_{MP2} + E_{def}$] of DMPImCl complex from the isolated ions. BSSE corrected interaction energies at the MP2/6-311G* level [E_{MP2}] are shown in parentheses. E_{def} (deformation energy) is the increase of the energy of DMPIm upon deformation of the geometry in complex formation.

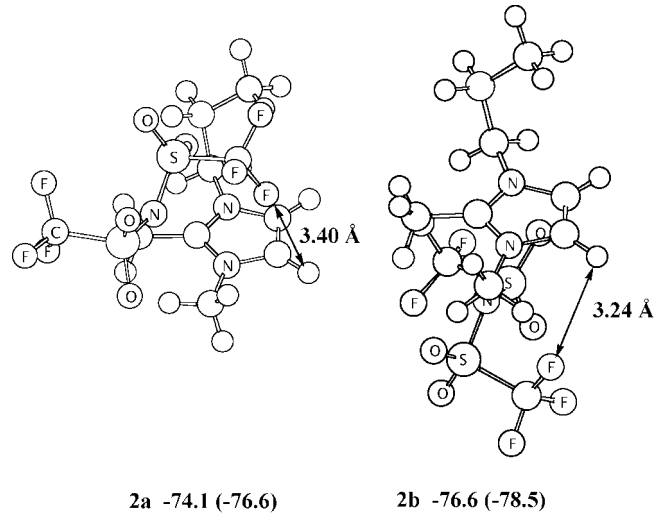

Figure 11. HF/6-311G** level optimized geometries and formation energies (E_{form}) of DMPImTFSA complex from isolated ions. See the text and the caption of Figure 10.

for imidazolium complexes with other anions.[37] The center of positive charge of the imidazolium ring is close to the midpoint between the two N atoms of the ring.[48] The complexes **1a** and **1b** are more stable than **1c**−**1e** due to shorter distances between the midpoint and the Cl^- than those in **1c**−**1e.** A similar calculation was reported for 1-butyl-2,3-dimethylimidazolium chloride.[49]

The geometries of DMPImTFSA were optimized from two initial geometries, which were prepared from the optimized geometries for **1a** and **1b** by replacing the Cl with TFSA. The N atom of TFSA was placed at the position of Cl, and the optimized geometries (**2a** and **2b**) are shown in Figure 11. The E_{form} values for **2a** and **2b** are −74.1 and −76.6 kcal/mol. The large E_{form} shows that the TFSA anion also prefers to have close contact with DMPIm. The optimized geometries have short contacts between the C_5-H and a F atom of TFSA as shown in Figure 11.

Discussion

Bulk Diffusive Properties. The Arrhenius plots of the D values and the ionic conductivity in Figure 3a gave different curvatures. Ionic conductivity measures the transfer of the charged ions, while the NMR measurements reflect the weighted average of the charged and paired ions due to the fast exchange of ion pairing on an NMR time scale. The VFT-type fitting shown in Figure 3a gave T_0 values of about 145 (DMPIm) and 151 (TFSA) K from the D values and 178 K from the σ. The glass transition temperature was reported to be 192 K. Even if the VFT-type fitting of diffusion coefficients were possible, the meanings of the fitting parameters should be different from the ionic conductivity.

Figure 3b indicates that experimentally eq 2 holds between the viscosity and anion and cation diffusion coefficients and ionic conductivity in the temperature range between 10 and 80 °C. The Stokes radius a is approximated with the van der Waals radius calculated from molecular orbital methods.[46] The c values estimated by using a values for DMPIm (0.330 nm) and TFSA (0.325 nm)[45] were not sensitive to temperature and were almost 2.5 and 3.5 for DMPIm and TFSA, respectively, which are smaller than the theoretically predicted range.

Local Molecular Motions. We assume that the τ_c of α-CH_2 in the propyl side chain corresponds to the isotropic molecular reorientational rotation of DMPIm. Almost the same τ_c values were obtained for the CH_3 at the α-positions of the imidazolium ring. The contribution from intramolecular rotations of CH_3 or segmental motions in the α-CH_2 may be possible, but the effect is minor. The activation energies in Table 2 for the side chain protons are between 19 and 24 kJ/mol and the small differences relate to the differences in steric hindrance which is clearly indicated in the stable structure of DMPIm estimated by ab initio calculation. As shown in Figure 6, above 313 K it is possible to interpret the ^{1}H T_1 of imidazolium protons by the same τ_c. Thus, in the high-temperature range, the isotropic molecular motions of the cation DMPIm exist characterized by a single correlation time, which explains the major part of the observed ^{1}H T_1 for all protons. Although similar modes of molecular reorientations exist continuously at lower temperatures, additional relaxation mechanisms contributing to the relaxation of the imidazolium ring protons are implied. The apparent activation energies for C_4-H and C_5-H were about 3 kJ/mol between 303 and 253 K, and very small to be observed by NMR.

One possibility for the short ^{1}H T_1 of the C_4-H and C_5-H protons is the intermolecular dipolar interactions with CF_3 of the TFSA anion. Neutron diffraction measurements of imidazolium-based ionic liquids show that an imidazolium cation is surrounded by a few anions in ionic liquids.[50−52] The diffraction measurements of 1,3-dimethylimidazolium TFSA shows that the anion prefers to locate above the imidazolium ring.[52] The TFSA also locates above the ring in the optimized structures of the DMPImTFSA ion pair as shown in Figure 11. The interactions of the CF_3 groups of TFSA anion with the C_4-H and C_5-H of DMPIm cation are not very strong, as the negative charges on the fluorine atoms are not large.[53] However, the contacts of the fluorine atoms with the C_4-H and C_5-H are likely to occur in the DMPImTFSA ionic liquid due to the size and shape of TFSA. In the optimized geometries of DMPImTFSA (**2a** and **2b**), the C-H_5 has a close contact with an F atom of TFSA (3.40 and 3.24 Å, respectively) as shown in Figure 11. Therefore. it is likely that the intermolecular dipolar interactions are possible between the CF_3 and the imidazolium protons.

Another possibility is the planar−nonplanar conformational changes observed by Raman spectroscopy for 1-ethyl-3-methylimidazolium salts.[54] The twisted conformation is reported to be slightly stable by 2−4 kJ/mol. Usually, the conformational changes involving small energy differences are observed as averaged phenomena on the NMR time scale. It may be possible that the slow rate of the conformational changes at low temperature is involved in the relaxation of the C_4-H and C_5-H protons, since the dipole−dipole interactions between the ring and the alkyl protons contribute to the ^{1}H T_1 of C_5-H as shown in Figure 6.

The correlation times of CF_3 in Figure 5 were calculated under the unjustified assumption that the relaxation process results from the internal rotation of CF_3 under the extreme narrowing condition. The ^{19}F τ_c of the CF_3 at higher temperatures has values similar to the ^{1}H τ_c of the CH_3 in the propyl group, and gradually their difference increased with decreasing temperature. Since the assumptions were made to derive ^{19}F τ_c, the activation energies calculated from the ^{19}F T_1 observed are given in Table 2. The thermal activation is smaller in the lower temperature range, similar to the C_4-H and C_5-H. The short-time approaches between DMPIm and TFSA in specified positions by electrostatic interactions can affect the ^{1}H and ^{19}F NMR relaxation process at lower temperatures.

The ^{1}H τ_2 and Diffusion Coefficient. The isotropic molecular overall reorientational correlation time τ_2 is related to the bulk viscosity η by the SED relation as

$$\tau_2 = \frac{V\eta}{kT} \tag{11}$$

where V is the effective molecular volume. From eq 2, $\eta = kT/c\pi aD$ and $\tau_2 = 4a^2/3cD$. It must be noted that D is the translational diffusion coefficient and not the rotational diffusion coefficient defined in the original SED relationship. Using the viscosity measured, the calculated τ_2 was 3.5×10^{-9} s (3.5 ns) at 298 K for DMPIm, which is much longer than the τ_c (3.2×10^{-10} s (320 ps)) determined by ^{1}H T_1 at the same temperature. There are a few studies on the τ_2 in RTILs. The solute rotation of 4-aminophthalimide ($C_8H_6N_2O_2$) in $BMImPF_6$ at 298 K was reported to be 8.7 ns from ESR measurements.[55] The smaller solutes of D_2O and C_6D_6 gave viscosity-dependent τ_2, and at 343 K the values were 62 and 119 ps in $BMImPF_6$ and 486 and 663 ps in BMImCl, respectively, studied by ^{2}H NMR.[56] The ion rotation in $BMImNO_3$ was reported to depend on the viscosity in the wide temperature range, and τ_2 was determined from by the optical heterodyne-detected Kerr effect (OHD-OKE) measurements to be about 650 ps around 295 K.[57] It is not certain that the experimental τ_2 values correspond to a full molecular rotation of 360°. Many papers have been published on the connection between the translational SE and rotational SED relations,[58] but experimentally it is difficult to obtain rotational diffusion coefficients.

Generally the ^{1}H dipole−dipole relaxation mechanism reflects any motion where the dipolar axis changes direction and does not guarantee the rotation of the whole molecule. The obtained τ_c values are too short to relate with the SED model. The analysis of the ^{1}H and ^{13}C T_1 values indicates that fast isotropic reorientational molecular motions exist, and we assumed that such motions are small angle reorientational motions of DMPIm. If the τ_2 value calculated from experimental η and D corresponds to a 360° rotation, the angles for the molecular reorientation (τ_c from T_1) were calculated and are plotted versus temperature in Figure 12. The molecular rotational amplitude becomes smaller at lower temperatures. The slope versus temperature changes about 40 °C. The molecular isotropic rotation of DMPIm can be pictured by the small angle reorientation of the whole molecule, and the flip amplitude changes from about 20°

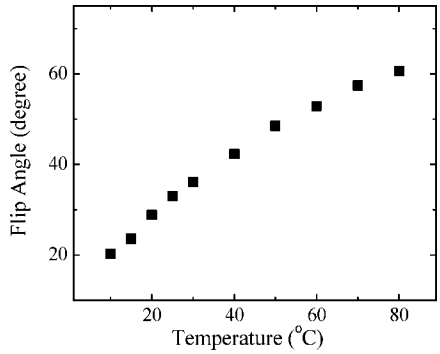

Figure 12. Temperature dependence of the flip angle of the isotropic reorientational molecular rotation of DMPIm assumed from τ_c (^{1}H T_1) and τ_2 (calculated from D_{DMPIm} and viscosity).

CHART 1: Stable Structures of DMPIm (top) and TFSA (bottom) Estimated by ab Initio Calculations

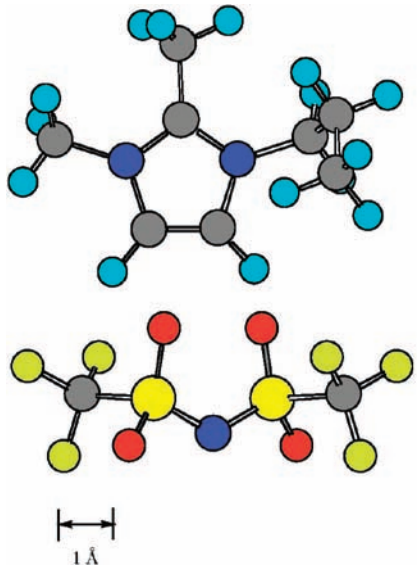

(at 10 °C) to 60° (at 80 °C). Fast intramolecular motions take place simultaneously such as CH_3 three-axis rotation, CH_2 segmental motions, and conformational changes of the imidazolium ring. A trial calculation of the rotational angle of TFSA gave smaller angles compared with DMPIm, but the mode of the motion of CF_3 is uncertain.

Conclusion

The electrochemical ion conduction of a RTIL, DMPImTFSA, showed different behaviors on temperature from the diffusion coefficients of the anion and cation measured by the PGSE-NMR method which are the averaged transfer of the whole ions without information on the charge of ions. In the higher temperature range the charged ions measured by ionic conductivity can be thermally activated easier than the whole ions. Since the temperature-dependent plots of the T_1 of ^{1}H NMR showed minimum points for DMPIm, the correlation times (τ_c) of the molecular motions were calculated. The ^{1}H T_1 minimum can afford directly the τ_c for the ^{1}H−^{1}H dipolar interaction, and the values were reasonable to interpret the T_1 of the ^{13}C NMR measured in the present study. Based on the classical SE and SED relations, an attempt was made to calculate the rotational angle for the reorientational DMPIm molecular motion in the temperature range between 283 and 353 K by using the translational diffusion coefficient, bulk viscosity, and τ_c values obtained from ^{1}H T_1. The amplitude of the rotation increases as the increase of temperature. Faster intramolecular motions exist, such as the segmental and rotational motions of alkyls and conformational changes of the imidazolium ring of the cation DMPIm. The anion TFSA molecular motions must have similar rates. The ion translational diffusion is much slower than molecular local motions.

Acknowledgment. The authors express their sincere thanks to Prof. W. S. Price for reading the manuscript critically and for fruitful discussion.

References and Notes

(1) *Electrochemical Aspects of Ionic Liquids*; Ohno, E., Ed.; Wiley: Hoboken, NJ, 2005.
(2) Zhang, S.; Sun, N.; He, X.; Lu, X.; Zhang, X. *J. Phys. Chem. Ref. Data* **2006**, *35*, 1475.
(3) http://ilthermo.boulder.nist.gov/ILThermo/mainmenu.uix.
(4) Noda, A.; Hayamizu, K.; Watanabe, M. *J. Phys. Chem. B* **2001**, *105*, 4603.
(5) Tokuda, H.; Hayamizu, K.; Ishii, K.; Susan, M. A. B. H.; Watanabe, M. *J. Phys. Chem. B* **2004**, *108*, 16593.
(6) Tokuda, H.; Hayamizu, K.; Ishii, K.; Susan, M. A. B. H.; Watanabe, M. *J. Phys. Chem. B* **2005**, *109*, 6103.
(7) Tokuda, H.; Ishii, K.; Susan, M. A. B. H.; Tsuzuki, S.; Hayamizu, K.; Watanabe, M. *J. Phys. Chem. B* **2006**, *110*, 2833.
(8) Tokuda, H.; Tsuzuki, S.; Susan, M. A. B. H.; Hayamizu, K.; Watanabe, M. *J. Phys. Chem. B* **2006**, *110*, 19593.
(9) Hayamizu, K.; Aihara, Y.; Nakagawa, H.; Nukuda, T.; Price, W. S. *J. Phys. Chem. B* **2004**, *108*, 19527.
(10) Hayamizu, K.; Tsuzuki, S.; Seki, S.; Ohno, Y.; Miyashiro, H.; Kobayashi, Y. *J. Phys. Chem. B* **2008**, *112*, 1189.
(11) Chung, S. H.; Lopato, R.; Greenbaum, S. G.; Shirota, H.; Castner, E. W., Jr.; Wishart, J. F. *J. Phys. Chem. B* **2007**, *111*, 4885.
(12) Nicotera, I.; Oliviero, C.; Henderson, W. A.; Appetecchi, G. B.; Passerini, S. *J. Phys. Chem. B* **2005**, *109*, 22814.
(13) Kanakubo, M.; Harris, K. R.; Suchihashi, N.; Ibuki, K.; Ueno, M. *J. Phys. Chem. B* **2007**, *111*, 2062.
(14) Stejskal, E. O. *J. Chem. Phys.* **1965**, *43*, 3597.
(15) Tanner, J. E. *J. Chem. Phys.* **1970**, *52*, 2523.
(16) Wu, D.; Chen, A.; Johnson, C. S. *J. Magn. Reson. A* **1995**, *115*, 260.
(17) Price, W. S.; Hayamizu, K.; Ide, H.; Arata, Y. *J. Magn. Reson.* **1999**, *139*, 205.
(18) Antony, J. H.; Mertens, D.; Dolle, A.; Wasserscheid, P.; Carper, W. R *Chem. Phys. Phys. Chem.* **2003**, 588.
(19) Carper, W. R.; Wahlbeck, P. G.; Antony, J. H.; Mertens, D.; Dolle, A.; Wasserscheid, P. *Anal. Bioanal. Chem.* **2004**, *378*, 1548.
(20) Carper, W. R.; Wahlbeck, P. G.; Dolle, J. *J. Phys. Chem. A* **2004**, *108*, 6096.
(21) Antony, J. H.; Dolle, A.; Mertens, D.; Wasserscheid, P.; Carper, W. R.; Wahlbeck, P. G. *J. Phys. Chem. A* **2005**, *109*, 6676.
(22) Heimer, N. E.; Wilkes, J. S.; Wahlbeck, P. G.; Carper, W. R. *J. Phys. Chem. A* **2006**, *110*, 868.
(23) Hayamizu, K.; Akiba, E.; Bando, T.; Aihara, Y. *J. Chem. Phys.* **2002**, *117*, 5929.
(24) Aihara, Y.; Sonai, A.; Hattori, M.; Hayamizu, K. *J. Phys. Chem. B* **2006**, *111*, 24999.
(25) Traficante, D. D. Relaxation: An Introduction. In *Encyclopedia of Nuclear Magnetic Resonance*; Grant, D. M., Harris, R. K., Eds.; Wiley: New York, 1996; Vol. 6, p 3988.
(26) Seki, S.; Kobayashi, Y.; Miyashiro, H.; Ohno, Y.; Usami, A.; Mita, Y.; Kihira, N.; Watanabe, M.; Terada, N. *J. Phys. Chem. B* **2006**, *110*, 10228.
(27) Seki, S.; Ohno, Y.; Kobayashi, Y.; Miyashiro, H.; Usami, A.; Mita, Y.; Tokuda, H.; Watanabe, M.; Hayamizu, K.; Tsuzuki, S.; Hattori, M.; Terada, N. *J. Electrochem. Soc.* **2007**, *154*, A173.
(28) Price, W. S.; Stilbes, P.; Jönsson, B.; Söderman, O. *J. Magn. Reson.* **2001**, *150*, 49.
(29) Hayamizu, K.; Price, W. S. *J. Magn. Reson.* **2004**, *167*, 328.
(30) Annat, G.; MacFarlene, D. R.; Forsyth, M. *J. Chem. Phys. B* **2007**, *111*, 9018.
(31) Weingatner, H. *Z. Phys. Chem. NF (Leipzig)* **1982**, *132*, 129.
(32) Frisch, M. J.; Trucks, G. W.; Schlegel, H. B.; Scuseria, G. E.; Robb, M. A.; Cheeseman, J. R.; Montgomery, J. A., Jr.; Vreven, T.; Kudin, K. N. ; Burant, J. C.; Millam, J. M.; Iyengar, S. S.; Tomasi, J.; Barone, V.; Mennucci, B.; Cossi, M.; Scalmani, G.; Rega, N.; Petersson, G. A.; Nakatsuji, H.; Hada, M.; Ehara, M.; Toyota, K.; Fukuda, R.; Hasegawa, J.;

Ishida, M.; Nakajima, T.; Honda, Y.; Kitao, O.; Nakai, H.; Klene, M.; Li, X.; Knox, J. E.; Hratchian, H. P.; Cross, J. B.; Bakken, V.; Adamo, C.; Jaramillo, J.; Gomperts, R.; Stratmann, R. E.; Yazyev, O.; Austin, A. J.; Cammi, R.; Pomelli, C.; Ochterski, J. W.; Ayala, P. Y.; Morokuma, K.; Voth, G. A.; Salvador, P.; Dannenberg, J. J.; Zakrzewski, V. G.; Dapprich, S.; Daniels, A. D.; Strain, M. C.; Farkas, O.; Malick, D. K.; Rabuck, A. D.; Raghavachari, K.; Foresman, J. B.; Ortiz, J. V.; Cui, Q.; Baboul, A. G.; Clifford, S.; Cioslowski, J.; Stefanov, B. B.; Liu, G.; Liashenko, A.; Piskorz, P.; Komaromi, I.; Martin, R. L.; Fox, D. J.; Keith, T.; Al-Laham, M. A.; Peng, C. Y.; Nanayakkara, A.; Challacombe, M.; Gill, P. M. W.; Johnson, B.; Chen, W.; Wong, M. W.; Gonzalez, C.; Pople, J. A. *Gaussian 03*, revision D.01; Gaussian, Inc.: Wallingford, CT, 2004.

(33) Møller, C.; Plesset, M. S. *Phys. Rev.* **1934**, *46*, 618.

(34) Head-Gordon, M.; Pople, J. A.; Frisch, M. J. *Chem. Phys. Lett.* **1988**, *153*, 503.

(35) Ransil, B. J. *J. Chem. Phys.* **1961**, *34*, 2109.

(36) Boys, S. F.; Bernardi, F. *Mol. Phys.* **1970**, *19*, 553.

(37) Tsuzuki, S.; Tokuda, H.; Hayamizu, K.; Watanabe, M. *J. Phys. Chem. B* **2005**, *109*, 16474.

(38) Metzler, R.; Klafter, J. *Phys. Rep.* **2000**, *339*, 1.

(39) Renner, U.; Schütz, G. M.; Vojta, G. Diffusion on Fractals. In *Diffusion in Condensed Matter*; Heitjans, P., Kärger, J., Eds.; Springer: Berlin, 2005; p 793.

(40) Kimmich, R. *Chem. Phys.* **2002**, *284*, 253.

(41) Hayamizu, K.; Aihara, Y.; Price, W. S. *J. Chem. Phys.* **2000**, *113*, 4785.

(42) Hayamizu, K.; Sugimoto, K.; Akiba, E.; Aihara, Y.; Bando, T.; Price, W. S. *J. Phys. Chem. B* **2002**, *106*, 547.

(43) Price, W. S.; Aihara, Y.; Hayamizu, K. *Aust. J. Chem.* **2004**, *57*, 1185.

(44) Abragam, A. *The Principles of Nuclear Magnetism*; Oxford: London, 1961.

(45) Ue, M.; Murakami, A.; Nakamura, S. *J. Electrochem. Soc.* **2002**, *149*, A1385.

(46) Edward, J. T. *J. Chem. Educ.* **1970**, *47*, 261.

(47) Levy, G. C.; Kerwood, D. J. Carbon-13 Relaxation Measurements: Organic Chemistry Applications. In *Encyclopedia of Nuclear Magnetic Resonance*; Grant, D. M., Harris, R. K., Eds.; Wiley: New York, 1996; Vol. 2, p 1147.

(48) Tsuzuki, S.; Tokuda, H.; Mikami, M. *Phys. Chem. Chem. Phys.* **2007**, 4780.

(49) Hunt, P. A. *J. Phys. Chem. B* **2007**, *111*, 4844.

(50) Hardacre, C.; Holbrey, J. D.; McMath, S. E. J.; Bowron, D. T.; Soper, A. K. *J. Chem. Phys.* **2003**, *118*, 273.

(51) Hardacre, C.; McMath, S. E. J.; Nieuwenhuyze, M.; Bowron, D. T.; Soper, A. K. *J. Phys.: Condens. Matter* **2003**, *15*, S159.

(52) Deetlefs, M.; Hardacre, C.; Nieuwenhuyze, M.; Padua, A. A. H.; Sheppard, O.; Soper, A. K. *J. Phys. Chem. B* **2006**, *110*, 12055.

(53) van den Berg, J. A.; Seddon, K. R. *Cryst. Growth Des.* **2003**, *3*, 643.

(54) Umebayashi, Y.; Fujimori, T.; Sukizaki, T.; Asada, M.; Fujii, K.; Kanzaki, R.; Ishiguro, S. *J. Phys. Chem. A* **2005**, *109*, 8976.

(55) Ingram, J. A.; Moog, R. S.; Ito, N.; Biswas, R.; Maroncelli, M. *J. Phys. Chem. B* **2003**, *107*, 5926.

(56) Yasaka, Y.; Wakai, C.; Matubayashi, N.; Nakahara, M. *J. Chem. Phys.* **2007**, *127*, 104506.

(57) Cang, H.; Li, J.; Fayer, M. D. *J. Chem. Phys.* **2003**, *119*, 13017.

(58) Mazza, M. G.; Giovambattista, N.; Stanley, H. E.; Starr, F. W. *Phys. Rev. E* **2007**, *76*, 031203, and references therein.

JP802392T